

## Conference Paper

# Bismuth Molybdate-based Oxygen Ion Conductors: Synthesis and Properties

Z. A. Mikhaylovskaya<sup>1</sup>, E. S. Buyanova<sup>1</sup>, and S. A. Petrova<sup>2</sup>

<sup>1</sup>Institute of Natural Sciences and Mathematics, Ural Federal University, 620002 Ekaterinburg, Russia

<sup>2</sup>Institute of Metallurgy of Ural branch of RAS, Yekaterinburg, Russia, 620016 Ekaterinburg, Russia

## Abstract

The present research is devoted to the synthesis and investigation of properties and structure of Ba-, Mn-, S-, and P- substituted  $\text{Bi}_{26}\text{Mo}_{10}\text{O}_{69}$ . The complex oxides have been synthesized using conventional method. The samples were examined using XRPD, IR FT spectroscopy, Rietveld full profile structure refinement, SEM, laser diffraction, and densitometry. Photocatalytic properties were investigated at RhB oxidation under UV irradiation. Electrical conductivity was studied with impedance spectroscopy. As a result, the best samples of Ba-, Mn-, S-, and P- substituted  $\text{Bi}_{26}\text{Mo}_{10}\text{O}_{69}$  can be recommended as high ionic conductive materials.

**Keywords:** oxygen ion conductors, bismuth molybdate

Corresponding Author:

Z. A. Mikhaylovskaya  
zozoikina@mail.ru

Received: 14 September 2018

Accepted: 1 October 2018

Published: 14 October 2018

Publishing services provided by  
Knowledge E

© Z. A. Mikhaylovskaya et al. This article is distributed under the terms of the [Creative Commons Attribution License](#), which permits unrestricted use and redistribution provided that the original author and source are credited.

Selection and Peer-review under the responsibility of the ASRTU Conference Committee.

## 1. Introduction

The  $\text{Bi}_2\text{O}_3$ -based complex oxides show ion conductive, catalytic, ferroelectric, and magnetic properties [1-3], as well as different structure types, such as fluorite-related structures, pillar or layered Aurivillius phases, or one-dimensional phases [1-4]. The illustration of the last one is column-type compound  $\text{Bi}_{26}\text{Mo}_{10}\text{O}_{69-d}$  (also named as  $\text{Bi}_{13}\text{Mo}_5\text{O}_{34.5-d}$ ). The  $\text{Bi}_{26}\text{Mo}_{10}\text{O}_{69}$  has a unique structure containing  $[\text{Bi}_{12}\text{O}_{14}]_n$  columns,  $[\text{MoO}_m]$  polyhedra, and 'isolated' Bi ions.  $\text{Bi}_{26}\text{Mo}_{10}\text{O}_{69}$  crystallizes in monoclinic symmetry at the temperature above  $\sim 310^\circ\text{C}$ ; below this temperature it exhibits a triclinic distortion. The structure of the monoclinic form was described in [5] with following unit cell parameters:  $a = 11.74$ ,  $b = 5.80$ ,  $c = 24.79 \text{ \AA}$ ,  $\beta = 102.84^\circ$  with P2/c space-group symmetry. The monoclinic model also includes  $[\text{Bi}_{12}\text{O}_{14}]_n$  columns, 'isolated' Bi ions, and  $\text{MoO}_4$  tetrahedra; the total quantity of oxygen position being only 68 per one unit cell. The structure of triclinic form with additional oxygen position was suggested in [6]. It includes  $\text{MoO}_5$  polyhedra and  $\text{MoO}_5$ - $\text{MoO}_4$  chains.

## OPEN ACCESS

Ordinary substitution in  $\text{Bi}_{26}\text{Mo}_{10}\text{O}_{69}$  can be realized by doping molybdenum sublattice or 'isolated' bismuth positions resulting to the general formula  $\text{Bi}_{26-2x}\text{Me}_{2x}\text{Mo}_{10-2y}\text{Me}'_{2y}\text{O}_{69-d}$ . They exhibit one-dimensional oxygen-ionic conductivity at mediate temperatures and photocatalytic properties [5-7].  $\text{Bi}_{26}\text{Mo}_{10-2y}\text{Me}''_{2y}\text{O}_{69-\delta}(\text{Bi}_{13}\text{Mo}_{5-y}\text{Me}''_y\text{O}_{34\pm\delta})$  solid solutions were synthesized with 4 or 6 coordinated dopants [5] such as  $\text{Me}'' = \text{Li}, \text{Mg}, \text{Al}, \text{Si}, \text{Ge}$  [8];  $\text{V}, \text{P}, \text{W}$  [9], etc. The compounds with formulae  $\text{Bi}_{26-2x}\text{Me}'_{2x}\text{Mo}_{10}\text{O}_{69-\delta}(\text{Bi}_{13-x}\text{Me}'_x\text{Mo}_5\text{O}_{34\pm\delta})$  were described for 8-coordinated dopants [5], such as  $\text{Ln}$  [10] or  $\text{Ca}, \text{Sr},$  and  $\text{Ba}$  [9]. Double substituted  $\text{Bi}_{26}\text{Mo}_{10}\text{O}_{69}$  has been uncommon and was described, for example, for  $(\text{Ca}, \text{Sr})_2\text{Bi}_{24}\text{Mo}_8(\text{Cr}, \text{W})_2\text{O}_{68}$  [11]. Changes of physicochemical characteristics are both positive and negative results from these substitutions. The present work is devoted to synthesis, investigation, and comparison of Ba-, Mn-, S-, and P- substituted  $\text{Bi}_{26}\text{Mo}_{10}\text{O}_{69}$ .

## 2. Methods

The powders of  $\text{Bi}_{26-2x}\text{Mn}_{2x}\text{Mo}_{10}\text{O}_{69-d}$ ,  $\text{Bi}_{26-2x}\text{Ba}_{2x}\text{Mo}_{10}\text{O}_{69-d}$ ,  $\text{Bi}_{26}\text{Mo}_{10-2y}\text{S}_{2y}\text{O}_{69-d}$ , and  $\text{Bi}_{26}\text{Mo}_{10-2y}\text{P}_{2y}\text{O}_{69-d}$  ( $0.0 \leq x, y \leq 1$ ) solid oxides were synthesized by conventional solid state methods from initial oxides and ammonia salts. Stoichiometric amounts of oxides were weighed, ground in an agate mortar with the ethyl alcohol as a homogenizer, and pelleted using uniaxial press. The pellets were placed in the alumina crucibles on the 'powder bed', heated at 823 K for 48 h, and then quenched at air to room temperature. After following regrinding and re-pelletizing, the samples were once more reheated to 1123 K for 24 h and cooled slowly in air to room temperature over a period of approximately 12 h. The concentration ranges of solid solutions and crystal forms of substituted  $\text{Bi}_{26}\text{Mo}_{10}\text{O}_{69-d}$  were determined by XRPD. X-ray powder diffraction data were obtained on a Bruker Advance D8 diffractometer with a VANTEC1 detector,  $\beta$ -filtered  $\text{Cu K}\alpha$  radiation,  $\theta/\theta$  geometry,  $2\theta$  range  $5-70^\circ$ , in steps of  $0.0211^\circ$ , with an effective scan time of 1 s per step. For full profile refinement, the data were collected in the  $2\theta$  range  $5-133^\circ$  with an effective scan time of 1649 s per step. DIFFRAC<sup>Plus</sup> Eva with TOPAS, PDF4 (ICDD) database, and CELREF software was used for the phase analysis. Hydrostatic weighing was used for investigating density of ceramic pellets coated with a moisture-resistant coating. The volume porosity of ceramic samples was obtained by comparison experimental and theoretical (X-ray) density of the samples. The grain size of the powders was estimated by a nanoparticle size analyzer (Shimadzu SALD-7101). The morphology of powders and sintered ceramic samples was carried out using a JEOL JSM 6390LA with EDX-analyzer JED 2300. Photocatalytic properties of

$\text{Ca}_{1-3x}\text{Bi}_{2x}\text{O}_x\text{MoO}_4$  series were investigated for degradation of Rhodamine B (RhB) under UV irradiation. The UV experiments were conducted in a photochemical reactor made of a jacketed quartz tube. A medium-pressure mercury vapor lamp HPL-N (Philips) of 125 W was used as an illuminating source. Temperature of the solution was  $\sim 40^\circ\text{C}$  during experiment. The RhB solution concentration was 25 ppm with a catalyst loading of  $1\text{ kg/m}^3$ . Samples were collected at regular intervals for subsequent analysis by spectrophotometer Unico 2800 (552 nm). Impedance measurements were used for conductivity characterization. The samples were pelletized at 20 bar to yield pellets of 10 mm diameter and ca. 3–4 mm thick and sintered at 1123 K during 24 h. Pt electrodes were obtained by covering the end surfaces of pellets by suspension of  $\text{NH}_4(\text{PtCl}_6)$  in ethanol with following drying and decomposition to the Pt. The impedance measurements were carried out in the range of 523–1123 K on an Elins Z-3000 impedance spectrometer over the respective frequency ranges 3 MHz to 10 Hz. For analysis of impedance plots, the equivalent electrical circuits method was used (Zview software, Version 2.6b, Scribner Associates, Inc.).

### 3. Results

The forming of  $\text{Bi}_{26-2x}\text{Me}'_{2x}\text{Mo}_{10}\text{O}_{69-d}$  and  $\text{Bi}_{26}\text{Mo}_{10-2y}\text{Me}''_{2y}\text{O}_{69-d}$  solid solutions was observed up to  $x = 0.8$  for  $\text{Me}' = \text{Mn}$ ,  $x = 0.7$  for  $\text{Me}' = \text{Ba}$ ,  $y = 0.7$  for  $\text{Me}'' = \text{P}$ , and  $y = 0.6$  for  $\text{Me}'' = \text{S}$ . The electron microscopy measurement confirmed these homogeneity ranges. The low concentration of dopant ( $x, y < \sim 0.1-0.3$ ) leads to triclinic forms of doped  $\text{Bi}_{26}\text{Mo}_{10}\text{O}_{69-d}$ , high dopant content ( $x, y > \sim 0.1-0.3$ ) produces the stabilization of monoclinic form of  $\text{Bi}_{26}\text{Mo}_{10}\text{O}_{69-d}$ -based solid solutions. The unit cell parameters of doped  $\text{Bi}_{26}\text{Mo}_{10}\text{O}_{69-d}$  show a good correlation with Vegard's law within these ranges (Figure 1). For S-doped samples, the gap caused by changing of coordination is observed at the curves of unit cell parameters.

Refining of structure of  $\text{Bi}_{26-2x}(\text{Mn}, \text{Ba})_{2x}\text{Mo}_{10}\text{O}_{69-d}$  and  $\text{Bi}_{26}\text{Mo}_{10-2y}(\text{S}, \text{P})_{2y}\text{O}_{69-d}$  series gives strong information about substitution of isolated Bi positions by Mn or Ba and substitution of Mo positions by S and P. The IR FT spectra of  $\text{Bi}_{26}\text{Mo}_{10-2y}(\text{S}, \text{P})_{2y}\text{O}_{69-d}$  samples (Figure 2) show presence of  $\text{PO}_4$  and  $\text{SO}_4$  groups [12, 13]. On the contrary, additional absorption bands for the  $\text{Bi}_{26-2x}(\text{Mn}, \text{Ba})_{2x}\text{Mo}_{10}\text{O}_{69-d}$  series are not observed. The Mo–O at  $680-900\text{ cm}^{-1}$  and Bi–O vibrations at  $560-400\text{ cm}^{-1}$  are indexed by [14–16] and present at IR FT spectra of all the samples.

The grain size of powdered samples was determined by SEM and laser diffraction to be in the range of 1–20  $\mu\text{m}$ . At the following step of research, the samples of substituted

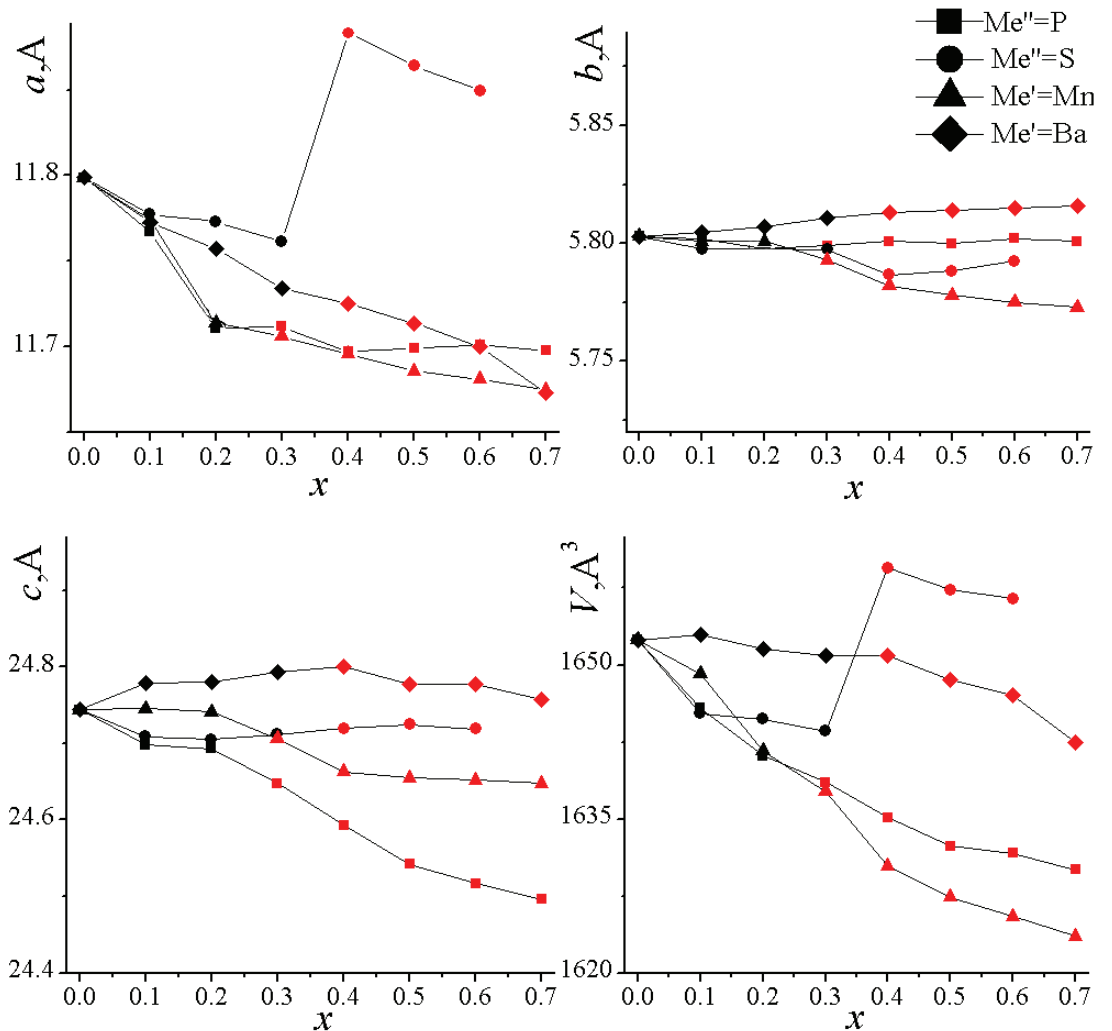


**Figure 1:** Unit cell parameters as a function of concentration of dopant in  $Bi_{26-2x}Me'_{2x}Mo_{10}O_{69-d}$  and  $Bi_{26}Mo_{10-2x}Me''_{2x}O_{69-d}$  compounds.

$Bi_{26}Mo_{10}O_{69-d}$  were pelleted and annealed at 1123 K for 12 hours. As an example, the images of the powder and surface and cross-section of  $Bi_{26}Mo_{10}O_{69-d}$ -based ceramics are shown in Figure 3. Scanning microscopy showed essential grain growth. Big grains (about dozens of microns) and isolated spherical pores are seen in massive ceramics, indicating the formation of dense. Hydrostatic weighing of the sintered ceramic pellets of the  $Bi_{26}Mo_{10}O_{69-d}$ -based ceramic revealed a high density of the sintered pellets. The magnitude of an experimental density reaches 97–99% of theoretical (X-ray) density, which corresponds to the 1–3% of porosity of the sintered ceramic pellets.

The electro-conductive properties of the ceramic samples of substituted  $Bi_{26}Mo_{10}O_{69-d}$  were investigated with the impedance spectroscopy. In general, complex plane plots were similar for all compounds. At the relatively high temperatures ( $\sim 873$ – $1123$  K), an impedance curve consisted of depressed unsymmetrical semi-circle (Figure 4(a)),

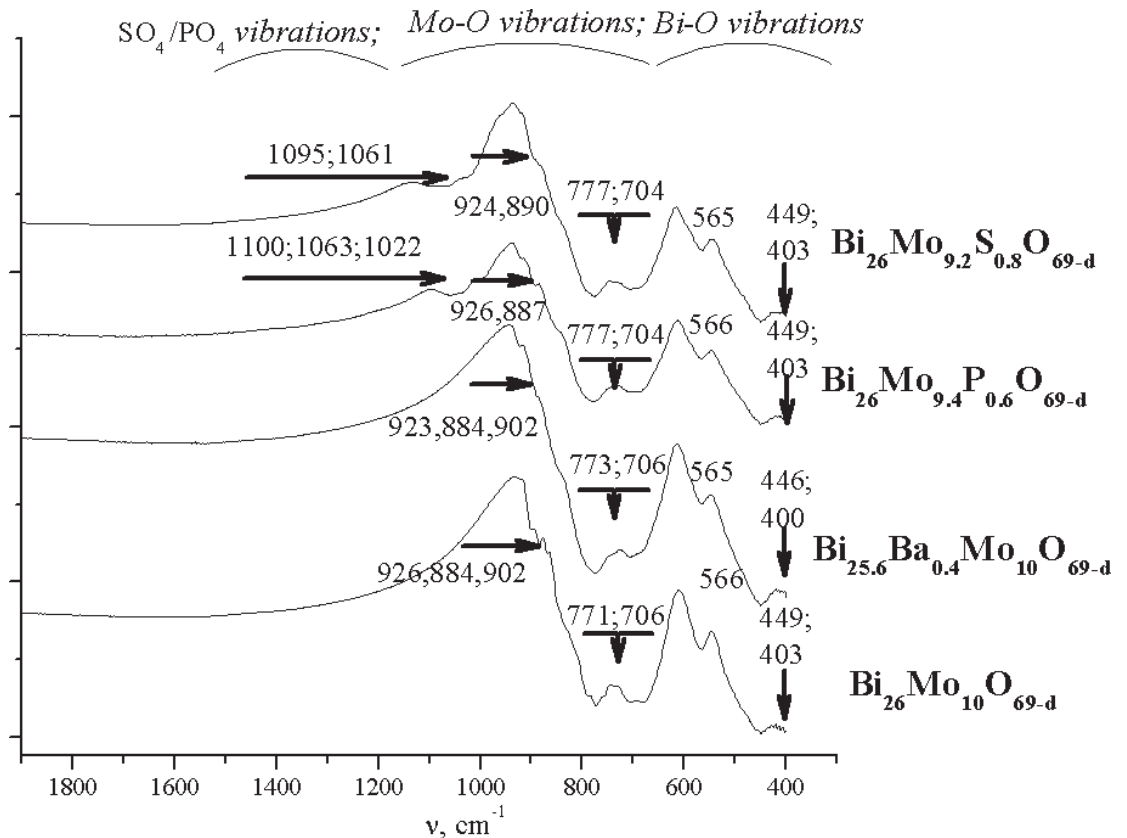
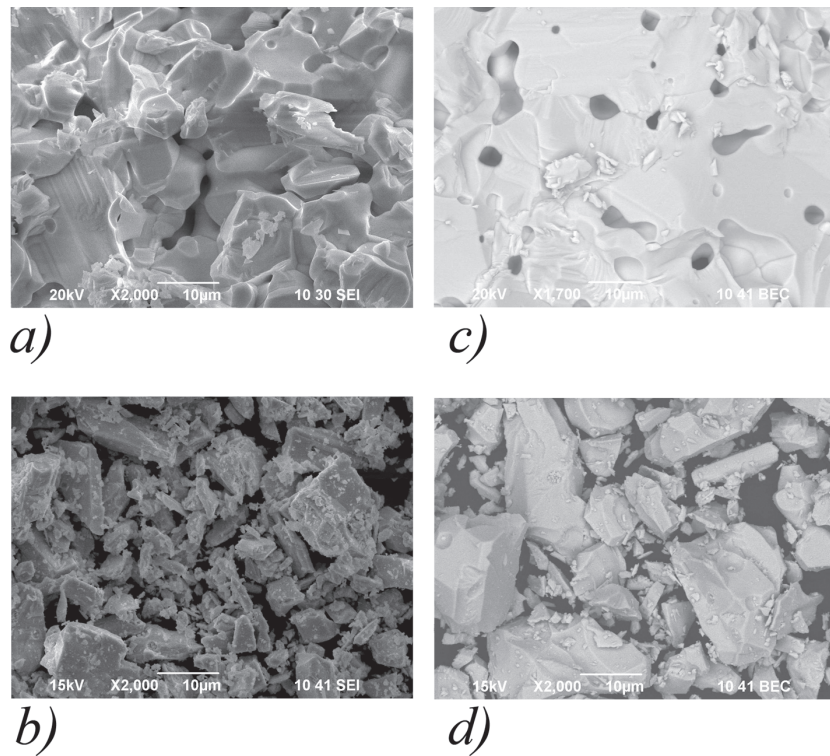


Figure 2: Typical IR FT spectra of Ba-, S-, and P- substituted  $\text{Bi}_{26}\text{Mo}_{10}\text{O}_{69}$  and parent compound.

TABLE 1: Conductivity values of the selected of Ba-, Mn-, S-, and P- substituted  $\text{Bi}_{26}\text{Mo}_{10}\text{O}_{69}$ .

Compound	$\sigma_{623K}, \text{S}\cdot\text{cm}^{-1}$	$\sigma_{1023K}, \text{S}\cdot\text{cm}^{-1}$
$\text{Bi}_{26}\text{Mo}_{10}\text{O}_{69-d}$	$6.45 \times 10^{-5}$	$6.90 \times 10^{-3}$
$\text{Bi}_{25.4}\text{Mn}_{0.6}\text{Mo}_{10}\text{O}_{69-d}$	$4.86 \times 10^{-6}$	$3.72 \times 10^{-3}$
$\text{Bi}_{25.6}\text{Ba}_{0.4}\text{Mo}_{10}\text{O}_{69-d}$	$6.30 \times 10^{-5}$	$8.31 \times 10^{-3}$
$\text{Bi}_{26}\text{Mo}_{9.8}\text{P}_{0.2}\text{O}_{69-d}$	$1.58 \times 10^{-4}$	$9.37 \times 10^{-3}$
$\text{Bi}_{26}\text{Mo}_{9.6}\text{S}_{0.4}\text{O}_{69-d}$	$1.57 \times 10^{-4}$	$7.77 \times 10^{-3}$
YSZ	$\sim 3 \times 10^{-5} - 3 \times 10^{-4}$	$1 \times 10^{-1} - 3.16 \times 10^{-2}$

which could be described by one resistor and two groups of parallel R-CPE connections (R was resistor, CPE was constant phase element). Capacity parameters of both CPE were  $\sim 10^{-5} - 10^{-4}$  F; therefore, R-CPE parallel connections corresponded to electrochemical processes at the electrodes [17]. The total resistivity of the sample corresponded to left intercept of spectra in its high frequency part. At relatively low temperatures ( $\sim 523 - 823$  K, Figure 4(b)), an impedance spectra consisted of slightly depressed semi-circle in the high frequency part associated to the straight line at the low frequencies. In this case, high frequency part represented the bulk resistivity of the sample [17]; low frequency parts of spectra represented diffusion processes and could be well



**Figure 3:** SEM-images of (a) & (c) ceramic and (b) & (d) powder of (a) Ba, (b) S, (c) Mn, and (d) P substituted  $\text{Bi}_{26}\text{Mo}_{10}\text{O}_{69}$ ; (a) & (c) secondary and (b) & (d) backscattering electrons, scale (c) 1:1700, (a), (b), & (d) 1:2000.

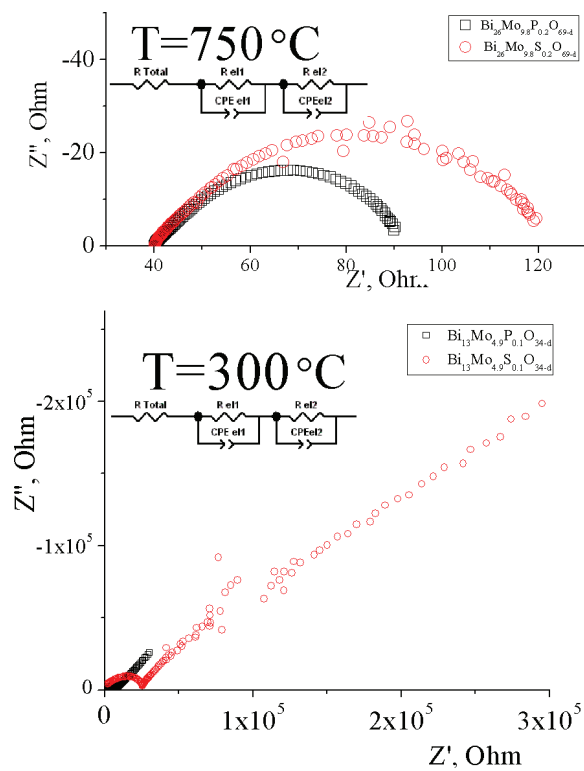


**Figure 4:** Typical impedance spectra of substituted  $\text{Bi}_{26}\text{Mo}_{10}\text{O}_{69}$  samples at the high and low temperature ranges.

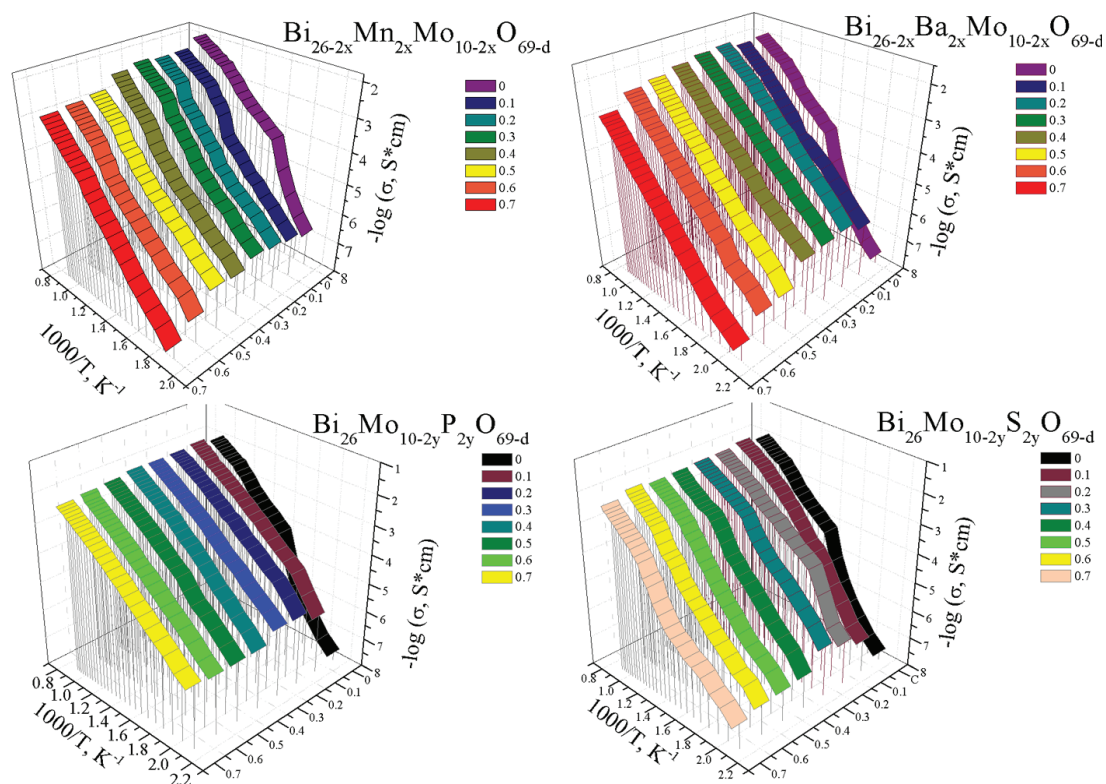


**Figure 5:** 3D thermal and concentration curves of conductivity of Ba-, Mn-, S-, and P- substituted  $\text{Bi}_{26}\text{Mo}_{10}\text{O}_{69-d}$ .

simulated using Warburg elements or by a pair of parallel R-CPE connections (with capacity parameters  $\sim 10^{-7}$ – $10^{-6}$  F and exponential parameter close to 0.5). As a result, the temperature and dopant concentration curves of conductivity were plotted (Figure 5). Samples with highest conductivity values are shown in Table 1. The conductivity values were comparable with the well-known ionic conductors, for example, YSZ [18].

Control experiments were carried out for RhB oxidation with and without catalyst at visible light (24 hours) and RhB oxidation with catalyst at dark (24 hours). Irreversible absorbance of RhB at catalysis or RhB oxidation under visible light was not detected. Investigation of the  $\text{Bi}_{26}\text{Mo}_{10}\text{O}_{69-d}$ -based solid solutions show a small decrease of the photocatalytic activity with dopant concentration. It was suggested that in doped  $\text{Bi}_{26}\text{Mo}_{10}\text{O}_{69-d}$  a raise of crystal symmetry from triclinic to monoclinic led to the slower adsorption and desorption processes. The examples of time dependences of degree of conversion and kinetic curves of RhB are shown in Figure 6. Concentration of RhB changes by Rate law  $C = C_0 \cdot \exp(-kt)$ , where  $C$  is concentration of RhB,  $C_0$  is initial concentration of RhB,  $k$  is reaction rate constant,  $t$  is time, as a result pseudo-first order reaction is observed. Results show that reaction rates decrease with dopant concentration by a factor of  $\sim 1$ – $1.5$ .

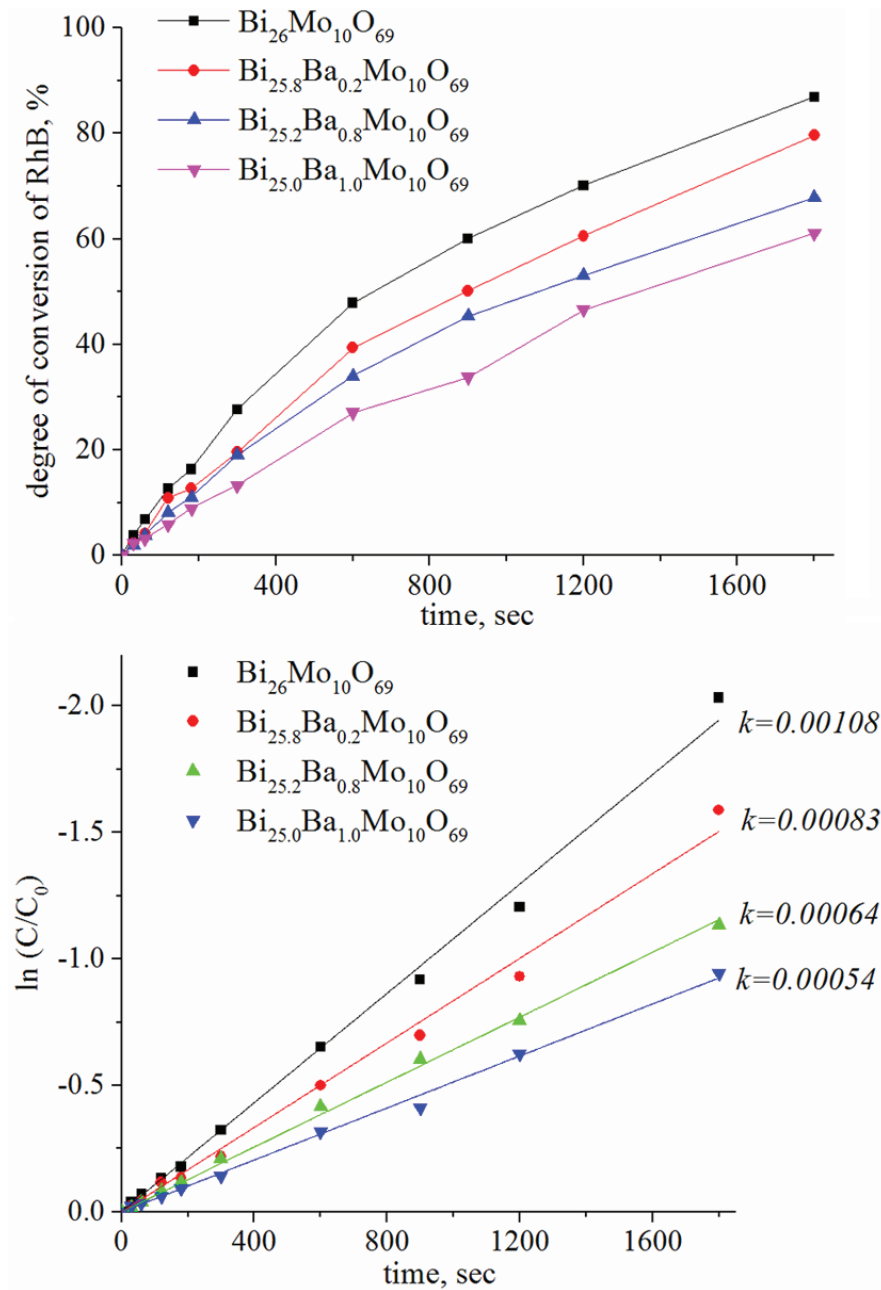


**Figure 6:** Typical time dependences of degree of conversion and kinetic curves of RhB for substituted  $\text{Bi}_{26}\text{Mo}_{10}\text{O}_{69}$ .

## 4. Conclusion

In the present research, the possibility of the substitution of  $\text{Bi}_{26}\text{Mo}_{10}\text{O}_{69}$  by Ba-, Mn-, S-, and P was shown. Doping of isolated Bi positions by Mn or Ba and substitution of Mo positions by S and P was detected. It was revealed that complex oxides were good ionic conductors and possible photocatalyst.

## Funding

This study was supported by RFBR (project N°16-33-60026).

## References

- [1] Vedrine, J. C., Coudurier, G., Forissier, M., et al. (1985). Catalytic properties of metallic oxides in partial oxidation reactions. *Materials Chemistry and Physics*, vol. 13, pp. 365–378.
- [2] Zhao, X., Xu, T., Yao, W., et al. (2009). Synthesis and photoelectrochemical properties of thin bismuth molybdate film with various crystal phases. *Thin Solid Films*, vol. 517, pp. 5813–5818.
- [3] Boivin, J-C. (2001). Structural and electrochemical features of fast oxide ion conductors. *International Journal of Inorganic Materials*, vol. 3, pp. 1261–1266.
- [4] Sharma, N., Macquart, R. B., Christensen, M., et al. (2009). Structure and crystal chemistry of fluorite-related  $\text{Bi}_{38}\text{Mo}_7\text{O}_{78}$  from single crystal X-ray diffraction and ab initio calculations. *Journal of Solid State Chemistry*, vol. 182, pp. 1312–1318.
- [5] Vannier, R. N., Mairesse, G., Abraham, F., et al. (1996).  $\text{Bi}_{26}\text{Mo}_{10}\text{O}_\delta$  solid solution type in the  $\text{Bi}_2\text{O}_3$ - $\text{MoO}_3$ - $\text{V}_2\text{O}_5$  ternary diagram. *Journal of Solid State Chemistry*, vol. 122, pp. 394–406.
- [6] Ling, C. D., Müller, W., Johnson, M. R., et al. (2012). Local structure, dynamics, and the mechanisms of oxide ionic conduction in  $\text{Bi}_{26}\text{Mo}_{10}\text{O}_{69}$ . *Chemistry of Materials*, vol. 24, pp. 4607–4614.
- [7] Muktha, B., Aarthi, T., Madras, G., et al. (2006). Substitution effect on the photocatalytic degradation by the series  $\text{A}_x\text{Bi}_{26-x}\text{Mo}_{10}\text{O}_{68-0.5y}$  (A = Ba, y = 0; A = Bi, La, y = 2): A Kinetic Study. *Journal of Physical Chemistry B*, vol. 110, pp. 10280–10286.
- [8] Bastide, B., Enjalbert, R., Salles, P., et al. (2003). Ionic conductivity of the oxide family  $\text{Bi}[\text{Bi}_{12}\text{O}_{14}(\text{Mo},\text{M})\text{O}_4]_5$  with M=Li, Mg, Al, Si, Ge and V. *Solid State Ionics*, vol. 158, pp. 351–358.
- [9] Vannier, R. N., Danze, S., Nowogrocki, G., et al. (2000). A new class of mono-dimensional bismuth-based oxide anion conductors with a structure based on  $[\text{Bi}_{12}\text{O}_{14}]_\infty$  columns. *Solid State Ionics*, vol. 136–137, pp. 51–59.
- [10] Galy, J., Salles, P., Rozier, P., et al. (2006). Anionic conductors  $\text{Ln}_{2/3}[\text{Bi}_{12}\text{O}_{14}](\text{MoO}_4)_5$  with Ln=La, Nd, Gd, Ho, Yb. Synthesis–spark plasma sintering–structure–electric properties. *Solid State Ionics*, vol. 177, pp. 2897–2902.

- [11] Muktha, B. and Guru Row, T. N. (2007). Crystal structure and ionic conductivity of the series  $A_2Bi_{24}Mo_8X_2O_{68}$  ( $A=Ca, Sr$  and  $Ba$  and  $X=Cr, W$ ). *Structural Chemistry*, vol. 18, pp. 195–202.
- [12] Smith, D. H. and Seshadri, K. S. (1999). Infrared spectra of  $Mg_2Ca(SO_4)_3$ ,  $MgSO_4$ , hexagonal  $CaSO_4$ , and orthorhombic  $CaSO_4$ . *Spectrochimica Acta Part A*, vol. 55, no. 4, pp. 795–805.
- [13] Hea, X., Guan, M., Lian, N., et al. (2010). Synthesis and luminescence characteristics of  $K_2Bi(PO_4)(MO_4):Eu^{3+}$  ( $M=Mo, W$ ) red-emitting phosphor for white LEDs. *Journal of Alloys and Compounds*, vol. 492, pp. 452–455.
- [14] Li, H. H., Li, K. W., and Wang, H. (2009). Hydrothermal synthesis and photocatalytic properties of bismuth molybdate materials. *Materials Chemistry and Physics*, vol. 116, no. 1, pp. 134–142.
- [15] Paul, T. and Ghosh, A. (2014). Structure and vibrational properties of  $La_{2-x}Bi_xMo_2O_9$  ( $0.05 < x < 0.4$ ) oxygen ion conductors. *Journal of Alloys and Compounds*, vol. 613, pp. 146–152.
- [16] Sammes, N. M., Tompsett, G., and Cartner, A. M. (1995). Characterization of bismuth lead oxide by vibrational spectroscopy. *Journal of Materials Science*, vol. 30, pp. 4299–4308.
- [17] Irvine, J. T. S., Sinclair, D. C., and West, A. R. (1990). Electroceramics: Characterization by impedance spectroscopy. *Advanced Materials*, vol. 2, no. 3, pp. 132–138.
- [18] Joo, J. H. and Choi, G. M. (2006). Electrical conductivity of YSZ film grown by pulsed laser deposition. *Solid State Ionics*, vol. 177, pp. 1053–1057.